Simultaneous control of growth mode and ferromagnetic ordering in Co-doped ZnO layers with Zn polarity

Hiroaki Matsui*
Center for the Promotion of Research on Nanoscience and Nanotechnology, Osaka University, Toyonaka, Osaka 560-8531, Japan

Hitoshi Tabata†
Institute of Scientific and Industrial Research, Osaka University, Osaka 567-0047, Japan
(Received 26 September 2006; revised manuscript received 13 November 2006; published 29 January 2007)

In this paper, we describe a new growth technique realizing the simultaneous control of growth mode and ferromagnetic ordering in Co-doped ZnO layers. Remarkable changes in growth occurred as a result of doping with Co ions. Exposure to O_2 plasma to generate an oxygen-rich atmosphere was indispensable for the fabrication of undoped ZnO layers given stabilization of the negatively charged growing surface in a two-dimensional (2D) mode. In contrast, the 2D mode of $Zn_{0.94}Co_{0.06}O$ layers was adequately retained in the absence of a plasma source, and was attributable to the covalence provided by the 3*d* character of Co ions compared with the 4*s* character of Zn ions. Spontaneous magnetization of $Zn_{0.94}Co_{0.06}O$ layers was closely correlated with the number of free electrons, which was controlled by the activation energy of donor levels. This was also confirmed for O-polar $Zn_{0.94}Co_{0.06}O$ layers. Ferromagnetic (FM) ordering was observed at n_e values close to the Mott transition and led to hopping conduction between shallow donor bands. However, levels of $p(O_2)$ below 10^{-6} mbar that yielded FM ordering generated a pitted surface and led to crystalline deterioration. Given our understanding of the formation mechanism of pits, we applied a periodic oxygen pressure-modulated epitaxy that resulted in the coherent growth of Co-doped ZnO layers with a 2D mode. This specific growth was effective in producing pit-free surface uniformities over large areas that maintained FM ordering.

DOI: 10.1103/PhysRevB.75.014438 PACS number(s): 47.54.Jk, 91.60.Pn, 47.54.De, 96.25.Ln

I. INTRODUCTION

Zinc oxide (ZnO) in binary systems has attracted intense interest with regard to the quantum confinement of carriers and excitons using quantum heterostructures,[1,2] the control of *n*-type and *p*-type conductivity,[3] and self-organized surface nanostructures.[4,5] Spintronics centered on III-V systems such as GaAs (Ref. 6) have recently emerged as a branch of nanoelectronics concerning the simultaneous manipulation of electrons and spin that could find uses in the form of diluted magnetic semiconductors (DMS). In ZnO-related materials, much interest has centered on magnetic functionality in Co-doped ZnO which possesses a large Faraday effect due to a strong *s*, $p-d$ interaction[7,8] and ferromagnetic properties with a high Curie temperature.[9,10] Many researchers have focused on elucidating the origin of ferromagnetic ordering in $Zn_{1-x}Co_xO$ using experimental and theoretical approaches.[11–13] Recent studies concerning magneto-optics and magnetotransport in $Zn_{1-x}Co_xO$ layers have reported an interaction between carrier and localized Co spins.[14–17]In our work, a correlation between ferromagnetic saturation magnetization and the concentration of free electrons was observed. We consider that $Zn_{1-x}Co_xO$ is of particular interest in investigations concerning the enhancement of quantum heterostructures derived from a coupling between spin and carriers. However, the growth control of layer deposition for a two-dimensional (2D) mode has seldom been reported for $Zn_{1-x}Co_xO$ layers despite its practical use in applications such as spintronics.

Homoepitaxy allows for the selection of a variety of growth directions that play an important role in determining various characteristics of grown layers. 2D growth for a sharp heterointerface is suitable for layer growth along the Zn polarity. Thus far, we have studied homoepitaxial growth of ZnO (Ref. 18) and have succeeded in fabricating high-quality $Mg_xZn_{1-x}O/ZnO$ multiquantum wells (MQWs) along the Zn-polar direction.[19] Additionally, surface nanostructures such as nanostripe arrays[20] and spatially-separated nanodots[21] have formed via self-assembly. Studies concerning homoepitaxial growth in ZnO have been widely undertaken by the industrial and academic sectors.[22,23] A final objective of our research is to examine the quantum size effect using MQW structures with $Zn_{1-x}Co_xO$ wells. Therefore, a detailed study of the growth mechanism in Zn-polar $Zn_{1-x}Co_xO$ layers is expected to contribute towards an elucidation of the origin of ferromagnetism and in a delineation of the nature of low-dimensional effects with MQW structures.

In this paper, the nature of layer growth in Zn-polar ZnO and Co-doped ZnO layers was studied. The substrate chosen was a hydrothermal ZnO (0001) single crystal since the homoepitaxy technique provides a more direct correlation between growth parameters and layer structure without external influences. This paper is divided into three parts. In Sec. III A, we initially present details of the growth origin of the 2D mode in ZnO layers prior to the growth of Co-doped ZnO layers, correlated closely with optical and electrical properties. The presence of an applied O_2 gas pressure influences the growth process and structural quality in $Zn_{0.94}Co_{0.06}O$ layers and produces a close relation between magnetization and electron concentration, as discussed in Sec. III B. Finally, periodic oxygen pressure-modulated growth of a $Zn_{0.94}Co_{0.06}O/ZnO$ superlattice was undertaken in an effort

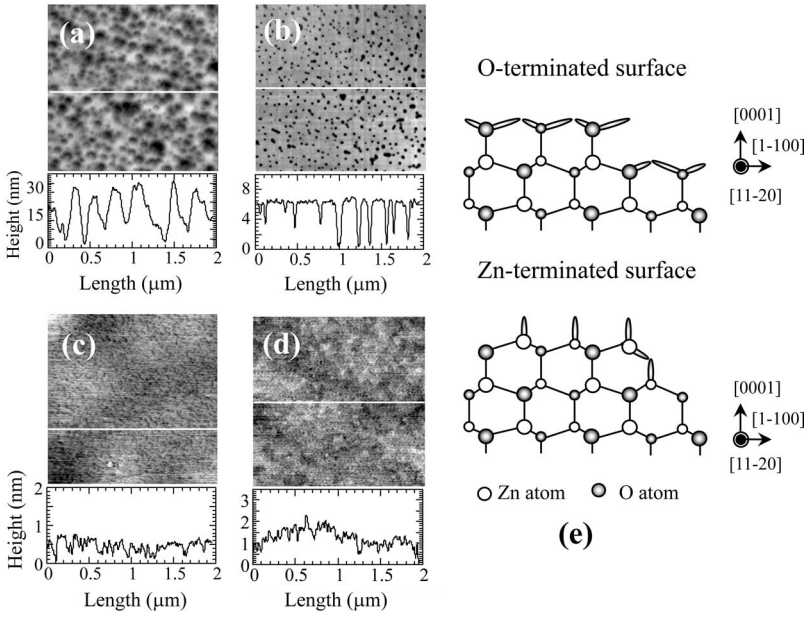

FIG. 1. AFM images of ZnO layers grown under a $p(O_2)$ of (a) 1.4×10^{-4}, (b) 1.4×10^{-5}, (c) 1.4×10^{-4}, and (d) 6.0×10^{-4} mbar. Oxygen flux was supplied by O_2 gas flow (a) or O_2 plasma exposure (b–d). (e) Schematic images of O- and Zn-terminated surfaces along the Zn-polar direction in ZnO lattice.

to resolve an obstacle in the Zn-polar growth of the Co-doped ZnO layer concerning simultaneous control of the growth mode and ferromagnetic (FM) ordering.

II. EXPERIMENTAL DETAILS

Zn-polar ZnO and $Zn_{0.94}Co_{0.06}O$ layers on thermally annealed ZnO (0001) substrates were grown using a laser molecular beam epitaxy (Laser-MBE) apparatus[24] with a radio-frequency (RF) plasma source. The O_2 gas pressure [$p(O_2)$] was changed from 6.0×10^{-4} to 6.0×10^{-8} mbar. The base pressure of the growth chamber was kept at 2.0×10^{-8} mbar. The input RF power was fixed at 280 W for operation in high-brightness mode. ArF excimer laser pulses ($\lambda=193$ nm, 3 Hz, and 50 mJ) were focused on ablation targets of ZnO single crystal (Eagle-Picher Co., 6*N*) and sintered ZnCoO(4*N*) ceramics located 4.5 cm from the substrates. The growth temperature (T_g) was fixed at a relatively low temperature of 400 °C in all experiments to limit secondary phases likely to be derived from Co oxides.[10]

The Co molar fraction was determined precisely with electron probe microanalysis (EPMA) using reference samples of pure ZnO (4*N*) and CoO (4*N*) single crystals. Details concerning application of the EPMA method for layers grown on ZnO substrates have been reported elsewhere.[19] The in-depth profile of Co concentration was investigated using secondary ion mass spectroscopy (SIMS). The surface morphology was examined by atomic force microscopy (AFM). Structural properties were characterized by high-resolution x-ray diffraction (HR-XRD) using a double-crystal monochromator and an analyzer crystal. Low-temperature photoluminescence (PL) spectroscopy was conducted at 10 K using a He-Cd laser ($\lambda=325$ nm) excitation source with a light power density of 2 mW. The Co (2*p*) core level and valence band spectra were observed using an x-ray photoemission spectrometer (XPS) equipped with a monochromatic Al $K\alpha$ x-ray source (1486.6 eV) and a concentric hemispherical analyzer. Magnetic measurements were performed using a Quantum Design SQUID magnetometer. The magnetic field was applied parallel to the layer plane. The substrate signal with diamagnetic property was subtracted using the slope of high fields above 2 T.This procedure gives the extrapolated spontaneous magnetization (M_s), but not the high-field slope. The electron concentration (n_e) and Hall mobility (μ_H) were measured using a Quantum Design PPMS apparatus with Hall measurements. The electrical resistivity of the semi-insulating ZnO substrates was in the order of 10^6 to 10^7 Ω.cm.

III. RESULTS AND DISCUSSION

A. Characterizations of ZnO layers

Figure 1 shows AFM images of 300 nm-thick ZnO layers grown under different conditions. The top surface of the layer grown under an O_2 gas flow of 1.4×10^{-4} mbar was completely covered by highly facetted pit features [Fig. 1(a)]. The layer grown under O_2 plasma exposure of 1.4×10^{-5} mbar also exhibited a pitted surface, although the layer appeared to be quite smooth between the pits. An O_2 plasma exposure in the range 1.4×10^{-4} to 6.0×10^{-4} mbar resulted in few pits with areas possessing a very flat surface [Figs. 1(c) and 1(d)]. The surface roughness of the layer was approximately 0.5 nm, a value corresponding to the *c*-axis length ($c=0.5205$ nm) in the ZnO lattice.

Figure 1(e) shows schematic images of O- and Zn-terminated surfaces along the [0001] direction in the ZnO lattice. The 2D mode in Zn-polar growth is indispensable for the deposition of a working layer under oxygen-rich conditions given stabilization by the negatively charged growth surface. Each surface atom on O- and Zn-terminated surfaces has one and three dangling bonds, respectively, suggesting that the O sticking coefficient on the Zn-terminated surfaces is lower than the Zn sticking coefficient on the O-terminated surfaces. The RF plasma source commonly generates excited

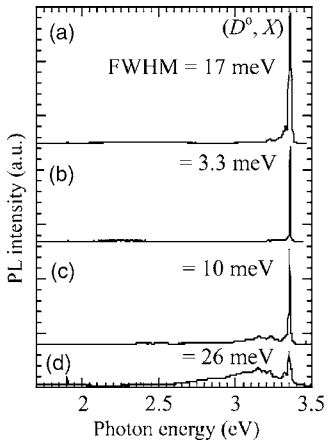

FIG. 2. Low-temperature PL spectra at 10 K for ZnO layers grown under a $p(O_2)$ of (a) 6.0×10^{-4}, (b) 1.4×10^{-4} (c) 1.4×10^{-5}, and (d) 1.4×10^{-4} mbar. Oxygen flux was supplied by O_2 plasma exposure (a–c) or O_2 gas flow (d).

atoms and molecules. For example, it is known that excited N^* atoms and N_2^* molecules enhance the N sticking coefficient on growing surfaces and increase the doping efficiency of nitrogen atoms into ZnO.[25] The presence of O_2 molecules results in a poor surface reaction due to a high dissociation energy (E_b) of 5.12 eV, which is similar to that of the N_2 molecule (E_b=9.76 eV). The rough surface on the layers grown under an O_2 gas flow is ascribed to incomplete O-terminated surfaces. In contrast,O_2 plasma exposure can supply excited O^* atoms to the growing surface. An O sticking coefficient enhanced by the excited O^* atoms contributes to the smooth conversion of a Zn-terminated surface to an O-terminated surface. This facilitates formation of a negatively charged growing surface and leads to stabilization of 2D growth. The observed morphological transitions are associated with changes in growth kinetics caused by a variation in the coverage of the ZnO surface by O atoms. This phenomenon is similar to the layer growth of Ga-polar GaN. Control of smooth GaN surface morphologies is obtained by complete surface coverage of excess Ga adatoms.[26]

Transport and optical properties are closely correlated with morphological changes, as detailed in Fig. 1. The layer with the heavily facetted pit surface exhibited a bounded exciton (D^o, X) emission at 3.351 eV, as well as a blue emission at 3.15 eV that was related to crystalline defects [Fig. 2(d)]. ZnO spontaneously exhibits n-type conductivity resulting from interstitial Zn (Zn_i) and oxygen vacancy (V_O). These intrinsic donors must be generated as major point defects evolving at relatively lower $p(O_2)$ regions. High n_e and low μ_H in the layers with the heavily facetted pit surface suggest that a large number of point defects are involved in the layer. Utilization of a plasma source revealed that the PL intensity of (D^o, X) increased markedly with suppression of the blue emission. A high optical quality was obtained in the layer grown under an O_2 plasma exposure of 1.4×10^{-4} mbar. The PL spectrum was dominated by a (D^o, X) emission at 3.357 eV, with a narrow linewidth of 3.3 meV [Fig. 2(b)]. Analysis of the growth of III-V compound semiconductors indicates an optimum flux ratio of III-V elements

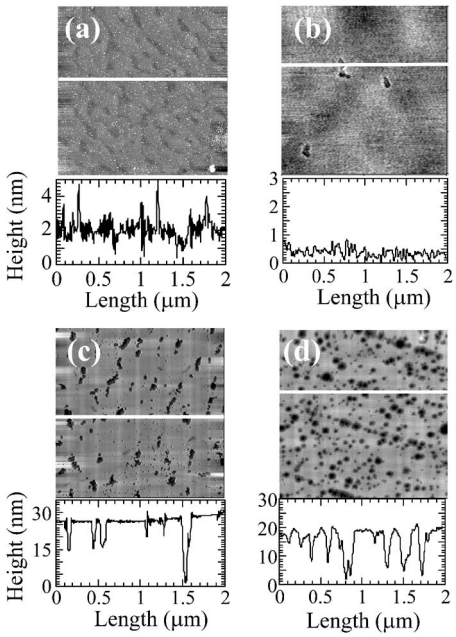

FIG. 3. AFM images of $Zn_{0.94}Co_{0.06}O$ layers grown under a $p(O_2)$ of (a) 1.4×10^{-4}, (b) 1.4×10^{-5}, (c) 1.4×10^{-6}, and (d) 1.4×10^{-7} mbar. Oxygen flux was only supplied by O_2 gas flow.

for the fabrication of high-quality samples. The MBE growth of ZnO revealed that stoichiometric flux conditions minimize the generation of crystalline defects in ZnO layers.[27] In this work, ZnO growth with a 2D surface under an O_2 plasma exposure of 1.4×10^{-4} mbar showed the highest μ_H ($\sim$84 $cm^2/V\,s$) and high-quality PL properties, being close to stoichiometric conditions. In contrast, a higher O_2 plasma exposure of 6.0×10^{-4} mbar resulted in deterioration of optical and electrical properties. The reduction in μ_H despite a lower n_e is presumably due to acceptorlike defects such as V_{Zn} acting as a dominant scattering center of free electrons. The layer grown under optimized conditions at 400 °C possesses a high n_e in the order of 1.2×10^{18} cm^{-3}, as supplied from shallow donors and is related to native defects derived from interstitial Zn (Zn_i) due to the low growth temperature. Incidentally, extrinsic impurities in the layer were in the order of 10^{16} cm^{-3}, as confirmed by SIMS analysis.

B. Characteristics of Co-doped ZnO layers

1. Surface and crystalline properties

Preliminary investigation under O_2 plasma exposure revealed that layer growth changed from a 2D to three-dimensional (3D) mode with increasing Co concentration, indicating that Co doping into ZnO markedly changed the growth mode compared with undoped ZnO. It was noticed that a layer growth of Co doped ZnO was deposited under an O_2 gas flow. AFM images of $Zn_{0.94}Co_{0.06}O$ layers grown under different O_2 gas pressures are shown in Fig. 3. The Co concentration was independent of $p(O_2)$ and was equivalent to 6%. The layer surface resulting from the highest $p(O_2)$ of 1.4×10^{-4} mbar showed slightly mounded structures with a roughness of 1.5 nm. A flat surface was obtained on the layer

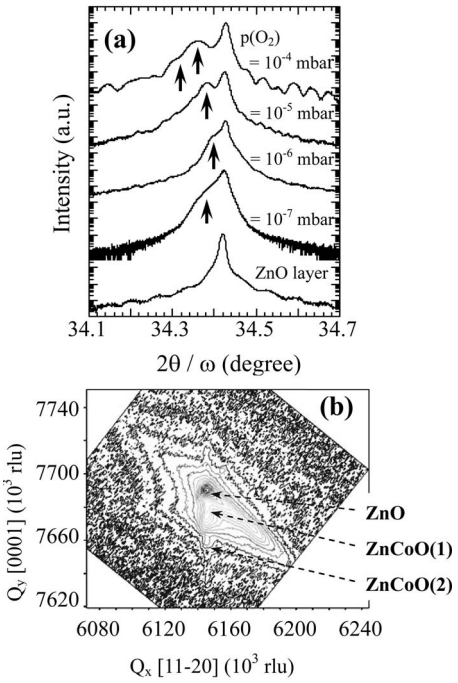

FIG. 4. (a) High-resolution $2\theta/\omega$ profiles of the (0002) reflection for $Zn_{0.94}Co_{0.06}O$ layers grown under different $p(O_2)$ with ZnO layers. (b) Reciprocal space mapping of the (11-24) reflection for $Zn_{0.94}Co_{0.06}O$ layers grown under a $p(O_2)$ of 1.4×10^{-4} mbar.

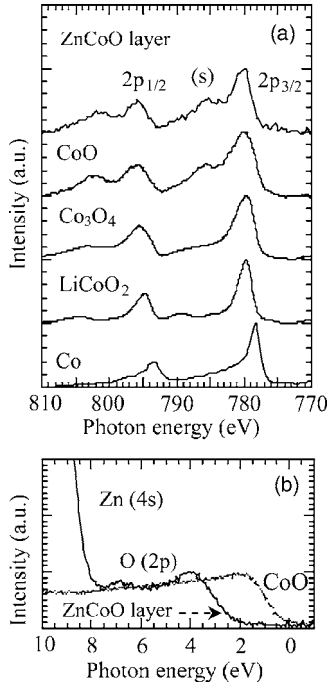

FIG. 5. (a) Co $2p$ core-level spectra of XPS for $Zn_{0.94}Co_{0.06}O$ layers and other Co oxides. (b) Valence band spectra of $Zn_{0.94}Co_{0.06}O$ layers (solid line) and CoO (dotted line). The $Zn_{0.94}Co_{0.06}O$ layer at a $p(O_2)$ of 1.4×10^{-6} mbar represents a typical sample.

grown under a $p(O_2)$ of 10^{-5} mbar, while lower $p(O_2)$ in the range 10^{-6} to 10^{-7} mbar resulted in pitted surfaces. Zn-polar growth of a Co-doped ZnO layer can maintain a 2D mode without O_2 plasma exposure, and is clearly different from the growth conditions applied to a ZnO layer in the absence of Co doping. This implies that Co atoms behave as a kind of surfactant on growing surfaces.

First-principles calculations for Co-doped ZnO materials have been suggested.[28] Co ions adhered to the ZnO surfaces are oxidized by adsorbed oxygen atoms, and then the covalent bonding around the Co ions is reinforced by the increase in formal charges. If Co ions are absent, the covalent bonding on the ZnO surface is weakened by oxygen adsorption. Thus, the presence of Co ions enhances oxygen adsorption onto the ZnO surface. If a similar process involving the role of Co ions takes place on the growing surface of a ZnCoO layer during laser-MBE, a negatively charged surface required for a 2D mode can be sufficiently realized under O_2 gas flow and results in a poor reaction on the growing surface. Section III A indicated that stabilization of the 2D mode in the undoped ZnO layer required O_2 plasma exposure for the generation of an oxygen-rich atmosphere. The marked change in growth conditions following Co doping in ZnO is related to the covalence provided by the $3d$ character of the transition metal compared with the $4s$ character of Zn.

Figure 4(a) shows the HR-XRD $2\theta/\omega$ patterns of $Zn_{0.94}Co_{0.06}O$ layers grown under different $p(O_2)$. No indications of a segregated phase could be detected. The highest $p(O_2)$ of 1.4×10^{-4} mbar caused a phase separation to $Zn_{1-x}Co_xO$ layers with varying Co concentration (x), as confirmed from reciprocal space mapping of the (11-24) reflection [Fig. 4(b)]. Phase-separated ZnCoO (wurtzite) layers grew coherently on ZnO substrates and showed an increase in c-axis length of 0.3% compared with bulk ZnO. It is known that Co-oxides segregate from ZnO ceramics by sintering in an oxygen atmosphere, resulting in varistor characteristics.[29] On the other hand, a reducing atmosphere resulted in nonsegregation of Co oxides. Thus, a layer growth of Co-doped ZnO under oxygen-rich conditions does not allow for dissolution of a large number of Co atoms into the ZnO. Separation into two types of ZnCoOphases doped with Co concentration within solubility limits may be stable under the highest $p(O_2)$. At a $p(O_2)$ of 1.4×10^{-5} mbar, $Zn_{0.94}Co_{0.06}O$ layers remained in a single phase with a $2\theta/\omega$ pattern clearly demonstrating pendellösung fringes. The fringes smeared out at a $p(O_2)$ of 1.4×10^{-6} mbar with appearance of the pit surface, and then disappeared completely at a $p(O_2)$ of 1.4×10^{-7} mbar following an increase in pit density. The origin of the fringes is based on interference between the layer surface and the layer/substrate interface. If lattice relaxation is introduced at the interface, the fringes are gradually weakened as the layer becomes thicker, and then disappear completely on a fully relaxed layer. A decrease in $p(O_2)$ causes strain relaxation, which is closely related to pit formation. Details of this mechanism will be discussed in Sec. III C.

2. Correlation with electrical and magnetic properties

Figure 5(a) shows typical XPS spectra of the $Zn_{0.94}Co_{0.06}O$ layer. The Co $2p$ core-level spectra exhibit a main Co $2p_{3/2}$ peak at 780.4 eV, accompanied by a satellite

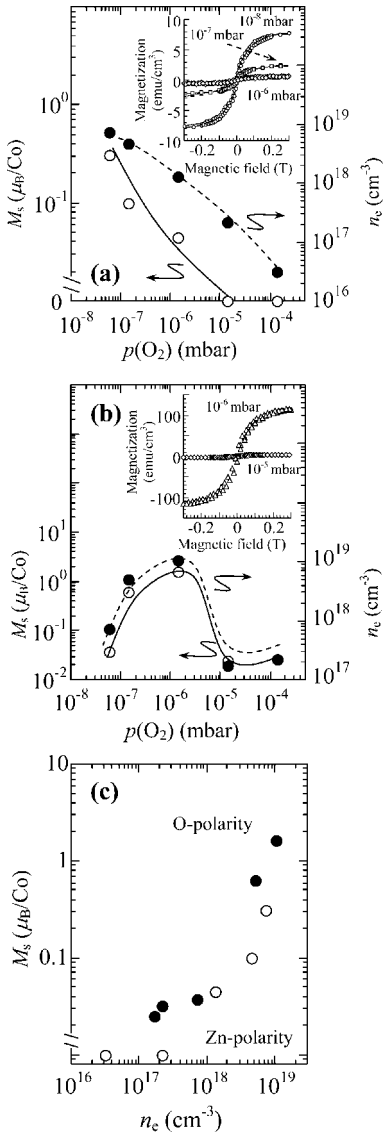

FIG. 6. (a) Dependence of M_s at 10 K (○) and n_e at 300 K (●) on $p(O_2)$ for Zn-polar $Zn_{0.94}Co_{0.06}O$ layers. The inset shows *M-H* hysteresis loops at 10 K for Zn-polar $Zn_{0.94}Co_{0.06}O$ layers grown under a $p(O_2)$ of 1.4×10^{-6} (◇), 1.4×10^{-7} (□), and 6.0×10^{-8} mbar (○). (b) Dependence of M_s at 10 K (○) and n_e at 300 K (●) on $p(O_2)$ for O-polar $Zn_{0.94}Co_{0.06}O$ layers. The inset shows *M-H* hysteresis loops at 10 K for O-polar $Zn_{0.94}Co_{0.06}O$ layers grown under a $p(O_2)$ of 1.4×10^{-5} (△) and 1.4×10^{-6} mbar (◇). (c) Logarithmic correlation between M_s at 10 K and n_e at 300 K for Zn polar (○) and O polar (●) $Zn_{0.94}Co_{0.06}O$ layers.

peak at 785.5 eV, with the Co $2p_{1/2}$ peak appearing at 795.6 eV (ΔE=15.5 eV).[30] There was little variation regarding spectra line shapes and peak binding energies with varying $p(O_2)$, indicating that the local electronic structure of Co ions is mostly independent of $p(O_2)$ within the resolution limits of XPS analysis. The Co $2p_{3/2}$ binding energy, Co$2p_{3/2}$-$2p_{1/2}$ separation and satellite structure differ from those of metallic Co and the oxides Co_3O_4 and $LiCoO_2$. The XPS spectrum of aCoO single crystal shows similarities to the layers since the Co ions in $Zn_{0.94}Co_{0.06}O$ possess the divalent high-spin state present in CoO crystals. It is possible that CoO at the layer surface is excluded by large differences in the valence band [Fig. 5(b)] and Co $2p$ line shapes. The Co $2p_{3/2}$ peaks of the CoO crystal are wider than the layers due to lattice effects, highlighting the fact that Co^{2+} ions are isolated within the $Zn_{0.94}Co_{0.06}O$ layers.

Figure 6(a) shows the correlation between M_s at 10 K and n_e at 300 K as a function of $p(O_2)$. $Zn_{0.94}Co_{0.06}O$ layers grown when $p(O_2)$ is above 10^{-5} mbar did not show spontaneous magnetization. A lower $p(O_2)$ of 10^{-6}, 10^{-7}, and 10^{-8} mbar produced hysteresis loops with M_s values of 0.72, 2.3, and 7.2 emu/cm^3 corresponding to 0.045, 0.10, and 0.31 μ_B/Co, respectively [inset of Fig. 6(a)]. The correlation between M_s and n_e as a function of $p(O_2)$ and FM ordering was also observed for O-polar $Zn_{0.94}Co_{0.06}O$ layers, as shown in Fig. 6(b) and the associated inset. $Zn_{0.94}Co_{0.06}O$ layers with O-polarity showed three-dimensional island growth by a spiral mode[31] and coherent growth on the ZnO substrate in all $p(O_2)$ regions. The electronic state of the Co ion retained a divalent state for all O-polar layers. FM ordering in O-polar layers was also affected by n_e, which was modulated with varying $p(O_2)$. It is worth noting from Fig. 6(c) that M_s at 10 K correlated closely with n_e at 300 K for Zn- and O polarity, indicating that the FM ordering is associated with an increase in n_e and represents an essential phenomenon that is independent of the polar direction and growth mode. Furthermore, a correlation between M_s and n_e values was found for polarities. As can be seen in Fig. 6(c), the relationship shows a scaling behavior that M_s is proportional to n_e^{α}, with α values of 0.82 and 1.15 for the data with Zn and O polarity, respectively. An increase in magnetization is observed at n_e regions close to the Mott transition of $n_M=6\times10^{18}$ cm^{-3} such that the electron motion in the shallow donor bands becomes "free." On the other hand, the lower n_e regions from 10^{16} to 10^{17} cm^{-3} are associated with a reduction in FM ordering. Thus, the FM ordering is closely linked with carrier concentration and affects the electronic structure in the band gap as discussed below.

Figure 7(a) shows n_e as a function of reciprocal temperature in $Zn_{0.94}Co_{0.06}O$ layers grown under different $p(O_2)$. By reducing $p(O_2)$, n_e at 300 K varied from 10^{16} to 10^{19} cm^{-3}. The carrier activation (E_d) behavior systematically evolves from a linear fitting of n_e near room temperature according to the following formula:[32]

$$n_e + N_A = \frac{N_D}{1 + g_d\left(\frac{n_e}{N_C}\right)\exp\left(\frac{E_d}{k_B T}\right)}, \quad (1)$$

where $g_d=g_1/g_0$ represents the factor with degeneracy of the unoccupied donor state $g_0=1$ and degeneracy of the occupied donor state $g_1=2$, assuming an *s*-like two-level system, and E_d and N_D represent the donor activation and donor concentration, respectively. For clarity, the quantity N_A represents the total number of deep acceptors acting as electron trapping centers in the host. Furthermore, $N_C=2(2\pi m^* k_B T/h^2)^{3/2}$ for ZnO denotes the effective density of states in the conduction band, where k_B and h are the Boltzmann and Plank constants, respectively, and m^* represents the electron effective mass in ZnO. E_d systematically

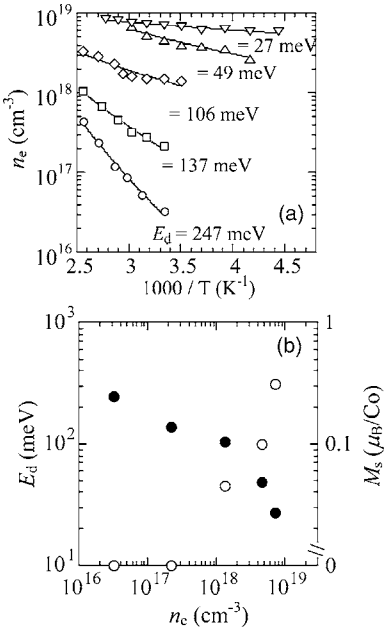

FIG. 7. (a) n_e as a function of reciprocal temperature for $Zn_{0.94}Co_{0.06}O$ layers grown under a $p(O_2)$ of 1.4×10^{-4} (○), (b) 1.4×10^{-5} (□), and (c) 1.4×10^{-6} (◇), 1.4×10^{-7} (△), and 6.0×10^{-8} mbar (▽). The solid line represents the theoretical fit according to Eq. (1). (b) E_d and M_s at 10 K in the $Zn_{0.94}Co_{0.06}O$ layers as a function of n_e at 300 K. (●) and (○) indicate E_d and M_s values, respectively.

decreased from 247 to 49 meV with decreasing $p(O_2)$, and N_D and N_A values were in the order from 10^{19} to 10^{20} cm^{-3} and 10^{17} cm^{-3} in all layers, respectively. The number of free electrons is not compensated by deep acceptors but is controlled by the activation energy of donor levels. Since Co ions in ZnO layers are in the divalent state, doped Co ions are considered a neutral dopant. Thus, n_e cannot be affected by doping with Co ions. The XPS results indicate that Co ions have actually been incorporated in the divalent state, and have no relation to $p(O_2)$. One theoretical investigation proposed the formation of Co_{Zn}-native defects in ZnO under an oxygen-rich atmosphere.[33] The decrease in n_e with increasing $p(O_2)$ was due to an increase in E_d following the generation of deep donor levels. Figure 7(b) shows E_d and M_s at 10 K in Zn-polar $Zn_{0.94}Co_{0.06}O$ layers as a function of n_e at 300 K. A large M_s was observed in the high n_e regions supplied from shallow donor levels, while an increase in E_d was suppressed following FM ordering with a decrease in n_e. This suggests that the high n_e around the Mott transition supplied from shallow donor levels plays an important role in maintaining FM ordering.

3. Discussion for an origin of FM ordering

The above results reveal that carrier conduction in the $Zn_{0.94}Co_{0.06}O$ layers is clearly related to FM ordering. In order to clarify the conduction mechanism of $Zn_{0.94}Co_{0.06}O$ layers with FM ordering grown under a $p(O_2)$ below 1.4×10^{-6} mbar, the temperature-dependent electrical conductivity (σ) was investigated, as shown in Fig. 8(a). The

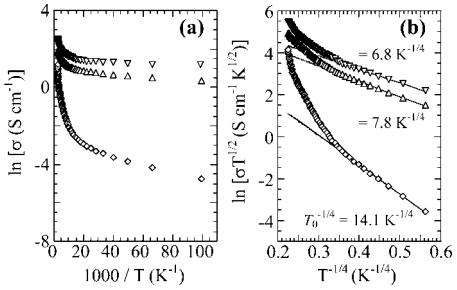

FIG. 8. (a) $\ln(\sigma)$ versus T^{-1} dependence for $Zn_{0.94}Co_{0.06}O$ layers grown under a $p(O_2)$ of 1.4×10^{-6} (◇), 1.4×10^{-7} (△), and 6.0×10^{-8} mbar (▽). (b) $\ln(\sigma T^{1/2})$ versus $T^{-1/4}$ dependence for $Zn_{0.94}Co_{0.06}O$ layers grown under a $p(O_2)$ of 1.4×10^{-6} (◇), 1.4×10^{-7} (△), and 6.0×10^{-8} mbar (▽). The solid lines represent the theoretical fit according to Eq. (2).

two mechanisms may be distinguished experimentally by operating in approximate temperature ranges due to the best-fitting functions for the lower (up to 75 K) and higher (from 75 to 390 K) temperature domains. At a lower temperature below 75 K, the weak temperature dependence implies that donor-based conduction is the prevailing transport mechanism since these temperature regions possess extremely low activation energy according to the Arrhenius equation. It is suggested that the conductivity mechanism obeys $T^{-1/4}$ and describes variable-range hopping (VRH) conduction by an over-lapping of the wave function of localized donor levels. All of the electronic states in the donor band are localized and the hopping process begins to dominate. The conductivity follows the VRH process of the Mott type, as given by the following equation:[34]

$$\sigma \propto T^{-1/2}\exp\left(\frac{-T_0}{T}\right)^{1/4}, \tag{2}$$

where T_0 is the characteristic hopping temperature. The $\ln(\sigma T^{1/2})$ vs $T^{-1/4}$ plots are shown in Fig. 8. The best agreement between experimental data and a theoretical fit of linear lines for layers grown under a $p(O_2)$ of 1.4×10^{-6}, 1.4×10^{-7}, and 6.0×10^{-8} mbar were obtained with $T_0^{-1/4}$ = 14.1, 7.8, and 6.8 K$^{-1/4}$, respectively, for low temperatures. For the Mott-type VRH conduction mechanism, T_0 and the hopping length R_{hop} are given by the following equations:[35]

$$T_0 = \frac{\beta}{k_B N(E_F)\xi^3} \tag{3}$$

and

$$R_{hop} = \left[\left(\frac{9}{8\pi}\right)\left(\frac{\xi}{k_B T N(E_F)}\right)\right]^{1/4}, \tag{4}$$

where β=18, ξ represents the localized length, and $N(E_F)$ reflects the density of states at the Fermi level. We may obtain the following relationship from an examination of Eqs. (3) and (4):

$$\frac{R_{\mathrm{hop}}}{\xi} = \left[\left(\frac{9}{8\pi\beta}\right)\left(\frac{T_0}{T}\right)\right]^{1/4}. \quad (5)$$

Using Eq. (5), the relation $R_{\mathrm{hop}}/\xi > 1$, as expected for VRH conduction, is satisfied with $T_0^{-1/4} = 14.1$, 7.8, and 6.8 $\mathrm{K}^{-1/4}$ for low temperatures. The layers exhibiting FM ordering possess carrier transport in an impurity band.

Super-exchange interactions with short-range order cannot be invoked for an explanation of the origin of FM ordering because FM ordering appears at a low concentration that is 6% below the percolation threshold ($x \sim 0.17$) associated with nearest-neighbor cation coupling in ZnO. From theoretical aspects,[36,37] Co doped into ZnO possesses large exchange splitting. Up-spin states of the 3*d* orbital are fully occupied and were set on the top of the valence band. On the other hand, partially occupied down-spin states are located near the Fermi level. Until now, common models of FM ordering in ZnO DMS materials suggested a strong coupling between magnetic ions and charge carriers in the vicinity of the Fermi level. If donor impurity such as Zn_i is introduced in the host lattice, shallow donor levels with low E_d are formed directly under the conduction band (CB) and then form an impurity band that causes a delocalization of carriers around the Mott transition. The Fermi level rises near the impurity band, resulting in strong hybridization and charge transfer from the impurity band to the empty 3*d* orbital of Co^{2+} ions near the Fermi level for FM ordering. This physical origin is derived from the spin-split impurity band model[13,38] and is suitable for our data in explaining that the transition of magnetic ordering from paramagnetic to FM depends on electron concentration. In contrast, deep donor levels in the band-gap are strongly localized charge carriers and suppress an itineration of electrons, resulting in low n_e and not FM ordering. Another possible origin is the Ruderman-Kittel-Kasuya-Yoshida (RKKY) interaction.[39]Shallow donors can provide free carriers into the CB consisting of a 4*s* orbital of Zn and lead to an *s-d* interaction for the generation of FM ordering between Co^{2+} ions through a high n_e above 10^{20} cm^{-3}. In the present case, the low n_e in the order of 10^{18} cm^{-3} is not sufficient to produce FM coupling on the basis of RKKY interaction. Therefore, it is suggested that a hopping motion of free electrons in the impurity band above the critical concentration is needed to mediate ferromagnetism in $Zn_{0.94}Co_{0.06}O$ layers and is closely related to a location of the empty 3*d* orbital near the Fermi level. The importance of shallow donor levels for FM ordering in Co-doped ZnO layers has been reported by Kittilstved *et al.*[40] In this work, we can assert that conditions which facilitate FM ordering are indispensable in forming shallow donor levels that lead to the hopping conduction at low temperature.

C. Periodic oxygen-pressure modulated epitaxy

At $p(O_2)$ levels below 10^{-6} mbar, Co-doped ZnO layers that showed FM ordering exhibited pitted surfaces. The pits observed in ZnO and $Zn_{0.94}Co_{0.06}O$ layers are ascribed to threading dislocations termed *V*-pit holes in accordance with $In_xGa_{1-x}N$ and GaN systems.[41] The strain effect is the primary cause of the formation of pits, and stacking faults generated by strain relaxation leads to the formation of pits.[42,43] It is speculated that pits do not form to contain the strain energy in the layer until a critical thickness is obtained, at which point it is favorable to release the stress by forming pits. This pit formation mechanism is consistent with the results of Figs. 3 and 4(a). Figure 9 shows AFM images of $Zn_{0.94}Co_{0.06}O$ layers with varying thickness under a $p(O_2)$ of 1.4×10^{-6} mbar. The pit density decreased with decreasing layer thickness and was reduced to orders of 10^7 cm^{-2} at a layer thickness of 10 nm.The pit density and layer thickness exhibited a logarithmic correlation. However, the n_e of a $Zn_{0.94}Co_{0.06}O$ layer with a thickness of 10 nm was 6.5×10^{18} cm^{-3}, demonstrating that the appearance of pit formation is not related directly to the high n_e. The free electrons caused by oxygen vacancies and interstitial Zn are not attributed to pit holes in the sub-micron scale, but to local point defects. Thus, the dependence of n_e on $p(O_2)$ clearly shows that $p(O_2)$ directly determines electron concentration in these layers during layer growth. Thus, 2D growth of the $Zn_{0.94}Co_{0.06}O$ layer at the lower $p(O_2)$ was obtained whilst maintaining the high n_e required for FM ordering with a decrease in the layer thickness. Furthermore, clear XRD fringes were observed with decreasing layer thickness, originating from coherent growth on the ZnO substrate. An explanation of these observations might suggest that a 2D mode in Zn polarity is retained even at lower $p(O_2)$ during the initial stage of $Zn_{0.94}Co_{0.06}O$layer growth. An incomplete covering of O atoms on the growing surface due to an oxygen-poor atmosphere results in growth instability of the 2D mode and leads to pit formation. The density of pits

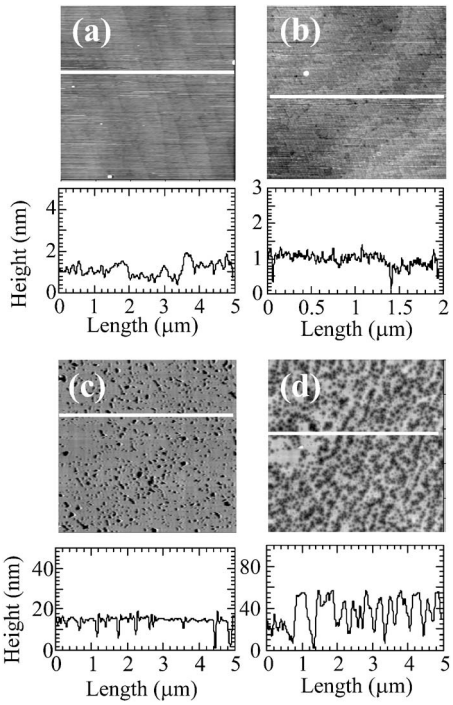

FIG. 9. AFM images of $Zn_{0.94}Co_{0.06}O$ grown under a $p(O_2)$ of 1.4×10^{-6} mbar with varying thickness. (a) 10 nm (pit density $\rho=2.0\times10^7$ cm^{-2}), (b) 24 nm ($\rho=2.3\times10^8$ cm^{-2}), (c) 90 nm ($\rho=4.0\times10^9$ cm^{-2}) and (d) 280 nm ($\rho>10^{10}$ cm^{-2}).

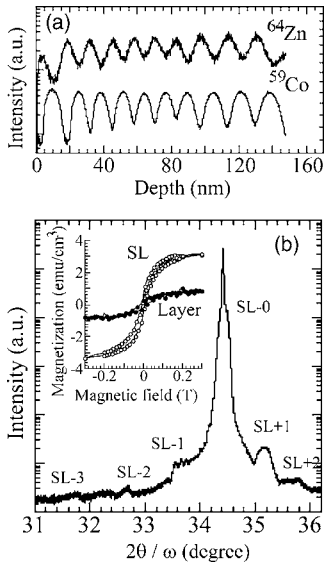

FIG. 10. (a) In-depth profiles of ^{64}Zn and ^{64}Co atoms using SIMS measurements. (b) High-resolution $2\theta/\omega$ profile of the (0002) reflection for the SL layer. The inset shows *M-H* hysteresis loops at 10 K for the SL (○) and $Zn_{0.94}Co_{0.06}O$ layers (●) grown under a $p(O_2)$ of 1.4×10^{-6} mbar.

rapidly increases as the layer thickness increases due to escalating strain relaxation.

We applied periodic oxygen pressure-modulated epitaxy to suppress pit formation on the Co-doped ZnO layer. This technique repeated the growth sequence of diluted magnetic $Zn_{0.94}Co_{0.06}O$ and non-magnetic ZnO layers under optimum growth conditions, which was also used to confirm FM ordering. A superlattice (SL) layer with ten-periods of a ZnO (4.4 nm)/$Zn_{0.94}Co_{0.06}O$ (8.2 nm) structure was grown at 400 °C under a $p(O_2)$ alternating between 1.4×10^{-4} and 1.4×10^{-6} mbar, corresponding to the ZnO and $Zn_{0.94}Co_{0.06}O$ layers. The RF plasma source was switched on and off during ZnO and $Zn_{0.94}Co_{0.06}O$ growth, respectively. The interval between growth at different $p(O_2)$ levels was 2 min. An SL period was evaluated using SIMS analysis [Fig. 10(a)], corresponding to an SL period (13 nm) estimated from the observed separation of the SL satellite. Figure 10(b) shows the (0002) diffraction pattern of the SL layer. The pronounced fringes and high-order satellite peaks suggest a high crystalline quality for the superlattice since any imperfection or composition inhomogeneity would decrease the phase coherence and eliminate the fringes. The ω-rocking curves of the SL satellite peak displayed a narrow linewidth of 48 arcsec. Furthermore, a smooth surface morphology without pits was obtained. The *M-H* curve at 10 K in the SL layer showed clear hysteresis, indicating that the SL is ferromagnetic at low temperatures [inset of Fig. 9(b)].

TABLE I. Electrical properties of ZnO layers grown under different conditions.

$p(O_2)$ (mbar)	RF plasma	n_e (cm^{-3})	μ_H (cm^2/V s)
(a) 1.4×10^{-4}	OFF	1.0×10^{19}	1.3
(b) 1.4×10^{-5}	ON	4.3×10^{18}	24
(c) 1.4×10^{-4}	ON	1.2×10^{18}	84
(d) 6.0×10^{-4}	ON	2.7×10^{17}	34

The M_s value of the SL was 3.2 emu/cm^3 and corresponded to $0.14\mu_B$/Co, which was three-times larger than that of the single layer grown under the same $p(O_2)$. FM ordering and 2D growth was simultaneously maintained by repeating a diluted magnetic $Zn_{0.94}Co_{0.06}O$ layer with high n_e followed by a nonmagnetic ZnO layer.

IV. CONCLUSION

The growth mechanism of Zn polarity in ZnO and $Zn_{0.94}C_{0.06}O$ layers was investigated. We observed dramatic changes in growth conditions as Co atoms were doped into ZnO. The 2D mode in $Zn_{0.94}C_{0.06}O$ layers was sufficiently retained in the absence of the O_2 plasma exposure required for layer growth of undoped ZnO, and is related to the covalence provided by the 3*d* character of the transition metal in comparison to the 4*s* character of Zn. The crystallinity, and donor levels that acted as compensating centers of free electrons, while a large M_s was observed because shallow donor levels were only formed in the electronic band gap, and contributed to hopping conduction between donor levels at low temperatures. To prevent pit formation and crystalline deterioration at low $p(O_2)$, we applied periodic oxygen-pressure modulated epitaxy for the fabrication of Co-doped ZnO layers. This method was effective in obtaining a highly crystalline pit-free surface that maintained FM ordering. This study has contributed to the area of spin-dependent physics and quantum heterostructures by presenting a clearer understanding of the growth mechanisms of Co-doped ZnO layers along the electrical (see Table I) and surface properties were strongly dependent on $p(O_2)$. Inparticular, we revealed that the M_s of $Zn_{0.94}Co_{0.06}O$ layers showed a correlation with electron concentration in the layers. FM ordering was markedly suppressed by formation of deep donor levels.

ACKNOWLEDGMENTS

This work was supported in part by a Grant-in-Aid for Young Scientists (No. 18760231) from the Japan Society for the Promotion of Science, and a research grant from The Murata Science Foundation (No. A61144).

*Email address: hiroaki32@sanken.osaka-u.ac.jp
†Present address: Department of Bioengineering, School of Engineering, The University of Tokyo, 7-3-1 Hongo, Bunkyo-ku, Tokyo 113-8656, Japan; email address: tabata@bioeng.t.u-tokyo.ac.jp

[1] A. Ohtomo, K. Tamura, M. Kawasaki, T. Makino, Y. Segawa, Z. K. Tang, G. K. L. Wong, Y. Matsumoto, and H. Koinuma, Appl. Phys. Lett. **77**, 2204 (2000).
[2] K. Koike, I. Nakashima, K. Hashimoto, S. Sasa, M. Inoue, and M. Yano, Appl. Phys. Lett. **87**, 112106 (2005).
[3] A. Tsukazaki, A. Ohtomo, T. Onuma, M. Ohtani, T. Makino, M. Sumiya, K. Ohtani, S. F. Chichibu, S. Fuke, Y. Segawa, H. Ohno, H. Koinuma, and M. Kawasaki, Nat. Mater. **4**, 42 (2005).
[4] H. Chik, J. Liang, S. G. Cloutier, N. Kouklin, and J. M. Xu, Appl. Phys. Lett. **84**, 3376 (2004).
[5] Y. Zhang, R. E. Russo, and S. S. Mao, Appl. Phys. Lett. **87**, 043106 (2005).
[6] G. A. Prinz, Science **282**, 1660 (1998).
[7] K. Ando, H. Saito, Z. Jin, T. Fukumura, M. Kawasaki, Y. Matsumoto, and H. Koinuma, J. Appl. Phys. **89**, 7284 (2001).
[8] W. Pacuski, D. Ferrand, J. Cibert, C. Depairs, J. A. Gaj, P. Kossacki, and C. Morhain, Phys. Rev. B **73**, 035214 (2006).
[9] K. Ueda, H. Tabata, and T. Kawai, Appl. Phys. Lett. **79**, 988 (2001).
[10] H. Saeki, H. Matsui, H. Tabata, and T. Kawai, J. Phys.: Condens. Matter **16**, S5533 (2004).
[11] K. Sato and H. Katayama-Yoshida, Jpn. J. Appl. Phys., Part 2 **40**, L334 (2001).
[12] M. H. F. Sluiter, Y. Kawazoe, P. Sharma, A. Inoue, A. R. Raju, C. Rout, and U. V. Waghmare, Phys. Rev. Lett. **94**, 187204 (2005).
[13] J. M. Coey, M. Vankatesan, and C. B. Fitzgerald, Nat. Mater. **4**, 173 (2005).
[14] P. Sati, R. Hayn, R. Kuzian, S. Régnier, S. Schäfer, A. Stepanov, C. Morhain, C. Deparis, M. Laügt, M. Goiran, and Z. Golacki, Phys. Rev. Lett. **96**, 017203 (2006).
[15] K. R. Kittlstved, D. A. Schwartz, A. C. Tuan, S. M. Heald, S. A. Chambers, and D. R. Gamelin, Phys. Rev. Lett. **97**, 037203 (2006).
[16] J. R. Neal, A. J. Behan, R. M. Ibrahim, H. J. Blythe, M. Ziese, A. M. Fox, and G. A. Gehring, Phys. Rev. Lett. **96**, 197208 (2006).
[17] Q. Xu, L. Hartmann, H. Schmidt, H. Hochmuth, M. Lorenz, R. Schmidit-Grund, C. Sturm, D. Spemann, and M. Grundmann, Phys. Rev. B **73**, 205342 (2006).
[18] H. Matsui, H. Saeki, T. Kawai, A. Sasaki, M. Yoshimoto, M. Tsubaki, and H. Tabata, J. Vac. Sci. Technol. B **22**, 2454 (2004).
[19] H. Matsui, N. Hasuike, H. Harima, and H. Tabata, J. Appl. Phys. **99**, 024902 (2006).
[20] H. Matsui and H. Tabata, Appl. Phys. Lett. **87**, 143109 (2005); J. Appl. Phys. **99**, 124307 (2006).
[21] H. Matsui, N. Hasuike, H. Harima, T. Tanaka, and H. Tabata, Appl. Phys. Lett. **89**, 091909 (2006).
[22] D. C. Look, D. C. Reynolds, C. W. Litton, R. L. Jones, D. B. Eason, and G. Cantwell, Appl. Phys. Lett. **81**, 1830 (2002).
[23] H. Kato, M. Sano. K. Miyamoto, and T. Yao, Jpn. J. Appl. Phys., Part 2 **42**, L1002 (2003).
[24] H. Matsui, H. Saeki, H. Tabata, and T. Kawai, J. Electrochem. Soc. **150**, G508 (2003); Jpn. J. Appl. Phys. **42**, 5494 (2003).
[25] H. Matsui, H. Saeki, T. Kawai, B. Mizobuchi, and H. Tabata, J. Appl. Phys. **95**, 5882 (2004).
[26] C. Poblenz, P. Waltereit, and J. S. Speck, J. Vac. Sci. Technol. B **23**, 1379 (2005).
[27] H. Kato, M. Sano, K. Miyamoto, and T. Yao, Jpn. J. Appl. Phys., Part 1 **42**, 2241 (2003).
[28] F. Oba, I. Tanaka, and H. Adachi, Jpn. J. Appl. Phys., Part 1 **38**, 3569 (1999).
[29] M. Okamoto, Y. Inoue, T. Kawahara, and J. Morimoto, Jpn. J. Appl. Phys., Part 1 **44**, 4461 (2005).
[30] M. Kobayashi, Y. Ishida, J. I. Hwang, T. Mizokawa, A. Fujimori, K. Mamiya, J. Okamoto, Y. Takeda, T. Okane, Y. Saitoh, Y. Muramatsu, A. Tanaka, H. Saeki, H. Tabata, and T. Kawai, Phys. Rev. B **72**, 201201 (2005).
[31] M. Kubo, Y. Oumi, H. Takaba, A. Chatterjee, A. Miyamoto, M. Kawasaki, M. Yoshimoto, and H. Koinuma, Phys. Rev. B **61**, 16187 (2000).
[32] R. Schaub, G. Pensl, M. Schulz, and C. Holm, Appl. Phys. A **34**, 215 (1984).
[33] F. Oba, T. Yamamoto, Y. Ikuhara, I. Tanaka, and H. Adachi, Mater. Trans. **43**, 1439 (2002).
[34] N. F. Mott, J. Non-Cryst. Solids **1**, 1 (1968).
[35] B. I. Shklovskii and A. L. Efros, in *Electronics Properties of Doped Semiconductors*, edited by M. Cardona (Springer-Verlag, Berlin, 1984).
[36] N. A. Spaldin, Phys. Rev. B **69**, 125201 (2004).
[37] E. C. Lee and K. J. Chang, Phys. Rev. B **69**, 085205 (2004).
[38] M. Venkatesan, C. B. Fitzgerald, J. G. Lunney, and J. M. D. Coey, Phys. Rev. Lett. **93**, 177206 (2004).
[39] A. F. Jabout, H. Chen, and S. L. Whittenburg, Appl. Phys. Lett. **81**, 2217 (2002).
[40] K. R. Kittilstved, W. K. Liu, and D. R. Gamelin, Nat. Mater. **5**, 291 (2006).
[41] H. K. Cho, J. Y. Lee, and G. M. Yang, Appl. Phys. Lett. **80**, 1370 (2002).
[42] T. L. Song, J. Appl. Phys. **98**, 084906 (2005).
[43] J. te Nijenhuis, H. F. J. M. van Well, M. M. G. Bongers, and L. J. Gilinh, Mater. Sci. Eng., B **52**, 17 (1998).